Facile access to cationic methylstannylenes and silylenes stabilized by E–Pt bonding and their methyl group transfer reactivity

Ramadoss Govindarajan,[a] Robert R. Fayzullin,[b] Shubham Deolka,[a] Eugene Khaskin,[a] Serhii Vasylevskyi,[a] Pavan K. Vardhanapu,[a] Shrinwantu Pal,[a] and Julia R. Khusnutdinova[a]*

[a]Okinawa Institute of Science and Technology Graduate University, 1919-1 Tancha, Onna-son, Okinawa, 904-0495, Japan.

[b]Arbuzov Institute of Organic and Physical Chemistry, FRC Kazan Scientific Center, Russian Academy of Sciences, 8 Arbuzov Street, Kazan, 420088, Russian Federation.

ABSTRACT: We describe a family of cationic methylstannylene and chloro- and azidosilylene organoplatinum(II) complexes supported by a neutral, binucleating ligand. Methylstannylenes MeSn:$^+$ are stabilized by coordination to Pt^{II} and are formed by facile Me group transfer from dimethyl or monomethyl Pt^{II} complexes, in the latter case triggered by concomitant B–H, Si–H, and H_2 bond activation that involves hydride transfer from Sn to Pt. A cationic chlorosilylene complex was obtained by formal HCl elimination and Cl^- removal from $HSiCl_3$ under ambient conditions. The computational studies show that stabilization of cationic methylstannylenes and cationic silylenes is achieved through weak coordination to neutral N-donor ligand binding pocket. The analysis of the electronic potentials, as well as the Laplacian of electron density, also reveals the differences in the character of Pt–Si vs. Pt–Sn bonding. We demonstrate the importance of a ligand-supported binuclear Pt/tetrel core and weak coordination to facilitate access to tetrylium-ylidene Pt complexes, and a transmetalation approach to the synthesis of $MeSn^{II}$:$^+$ derivatives.

Introduction

Since the groundbreaking discovery of stable carbene complexes of transition metals (TM), the coordination chemistry of their analogues, where the carbon is replaced by a heavier Group 14 element, has attracted intense interest in main-group chemistry.[1] Compared to a carbene, the heavier congeners are more likely to stabilize lower oxidation states and have a lower electronegativity.[1d, 2] The ability to act as both strong σ-donors and electrophiles (Lewis ambiphilicity) define the unique coordination properties of heavier tetrylenes (tetrel donor atom = Si, Ge, Sn, and Pb) as ligands for TM complexes, making them distinctly different from carbenes.[3] The high reactivity of stannylene and silylene complexes has been demonstrated in several recent bond activation processes via bimetallic TM−E cooperation, where a Sn or Si-based ligand plays a non-innocent role[4] and hydrogen migration processes[5] The intermediacy of silylenes has also been studied earlier in Glaser–Tilley hydrosilylation catalyzed by Ru complexes.[6] The accelerating effect of Sn^{II} additives is well-established in Group 10 metal/Sn bimetallic catalysis, including applications in hydroformylation,[7] cyclization/reductive coupling,[8], etc.,[9] with the formation of a Pt–Sn bond being invoked in some of these systems. Recent studies also proposed that tin(II) may play a role as a transmetalation acceptor from Group 10 metal alkyls, improving the stability of metal alkyl species towards β-hydride elimination.[9]

Among heavier Group 14 elements, the coordination chemistry of cationic tetrylium-ylidenes RE:$^+$ derivatives is especially intriguing as such compounds are expected to act as σ-donors forming a coordination bond to the metal, and at the same time, they are expected to show pronounced electrophilicity due to a positive charge and the availability of unoccupied *p*-orbitals.[1d] However, synthetic access to such species and their TM complexes remains challenging due to their high reactivity. Various strategies towards stabilization of such cationic RE:$^+$ species involve the utilization of rigid chelating ligands or sterically encumbered systems,[10] stabilization by N-heterocyclic carbenes (NHCs),[11] or inter/intramolecular coordination to Lewis bases[12] or Cp* ligands. [13] However, the number of reported TM complexes with cationic silylenes[14] and stannylenes[15] (including systems with multiple TM–Sn bonds[16]) remains limited.[1d, 4b] In the case of cationic organostannylenes, for example, the majority of TM complexes contain aryl–Sn^+ derivatives,[15b-d, 15f] while the synthesis of alkyl–Sn^+ complexes remains challenging.

Considering the important role of Sn and Si derivatives in Group 10 metal catalysis, we aimed to investigate bimetallic complexes containing Pt^{II} and a heavier Group 14 element, Sn or Si, using our recently developed, universal unsymmetrical "soft"-"hard" binucleating ligand scaffold **L** (Scheme 1).[17] Unexpectedly, complexation of Sn^{II} triggered facile methyl group transfer from Pt^{II} to Sn^{II} and generated a stable, cationic Me−Sn:$^+$ complex stabilized by a Sn−Pt bond and by Sn^{II} interactions with an N-binding pocket of the ligand. Moreover, we observed that methyl group transfer from the formally cationic monomethyl Pt^{II} to (dihydroxy)Sn^{II} core could be induced by Si−H, B−H, and H_2 activation to generate another type of Me−Sn:$^+$, this time bound to a platinum hydride. In search of new synthetic routes to cationic silylene complexes, we have also developed a new route to cationic X−Si:$^+$ complexes (X = Cl or N_3) with monomethyl Pt via formal HCl elimination from $HSiCl_3$ at room temperature, followed by halide exchange.

While alkyltin(IV) derivatives have often been used as transmetalating reagents in Pd-catalyzed Stille cross-coupling reaction[18] or stoichiometric transmetalation from

Group 10 metal to neutral dichlorotin(II),[9] the reactivity of cationic, low-valent stannylenes in transmetalation has not been previously established. This study provides the first evidence of facile Me group transfer from a Group 10 metal center to a cationic stannylene that is enabled by bimetallic cooperation. During the course of the study, we gained access to a new family of stable, cationic methylstannylene and silylene complexes with platinum(II) via new synthetic routes.

Scheme 1 Unsymmetrical binucleating ligand L and examples of cationic methylstannylene and silylene Pt^{II} complexes reported in this work.

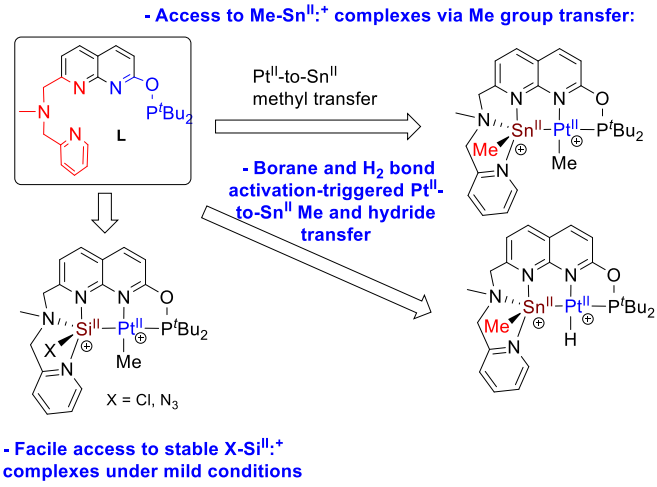

Results and Discussion

Methylstannylene Pt^{II} Complex Synthesis. The synthesis of the universal, unsymmetrical, binucleating ligand scaffold **L** has previously been reported by our group, where it was used for the selective formation of $PtMe_2$/M (M = Cu^{I} or Zn^{II}) complexes.[17a, 17c] Interestingly, in all previous examples of $PtMe_2$ complexation with Cu^{I} and Zn^{II}, only a weak interaction of one of the Pt–Me groups with Cu or Zn was observed, leading to bond elongation that depended on the metal's Lewis acidity, while complete transmetalation from Pt to Cu or from Pt to Zn has not been observed and both Me groups resided primarily on the Pt center.

In this work, we expanded the application scope of **L** to combine an organometallic Pt center with a main group element, Sn or Si. First, we treated a previously reported monometallic $PtMe_2$ precursor **1**[17a] with a Lewis acidic $Sn^{II}(OTf)_2$ salt containing weakly coordinating triflate anions in MeOH/H_2O solution at room temperature (RT). According to NMR spectroscopy, after 1 hour a mixture of two products, **2** and **3[OTf]$_2$**, was formed, which were characterized by distinct ^{31}P signals at 179.6 ppm ($^{1}J_{PtP}$ = 3498 Hz) and 183.5 ppm ($^{1}J_{PtP}$ = 3902 Hz) (Scheme 2a). The two products were easily separated due to their differing solubility profiles. Poorly soluble, colorless **2**, was obtained by precipitation from methanol and isolated in 58% yield, and well-soluble yellow product **3[OTf]$_2$** was obtained from the filtrate and isolated in 38% yield. Both complexes **2** and **3[OTf]$_2$** were characterized by ^{1}H, $^{13}C\{^{1}H\}$, $^{119}Sn\{^{1}H\}$, $^{195}Pt\{^{1}H\}$, and $^{31}P\{^{1}H\}$ NMR, UV-vis, and FT-IR spectroscopy, and electrospray ionization high-resolution mass-spectrometry (ESI-HRMS).

Scheme 2 (a) Synthesis of Pt–Sn complexes (isolated yields are shown in parentheses). (b) Reactivity of a model Pt complex in the absence of a ligand-supported Pt–Sn bonding, leading to exclusive protonolysis.

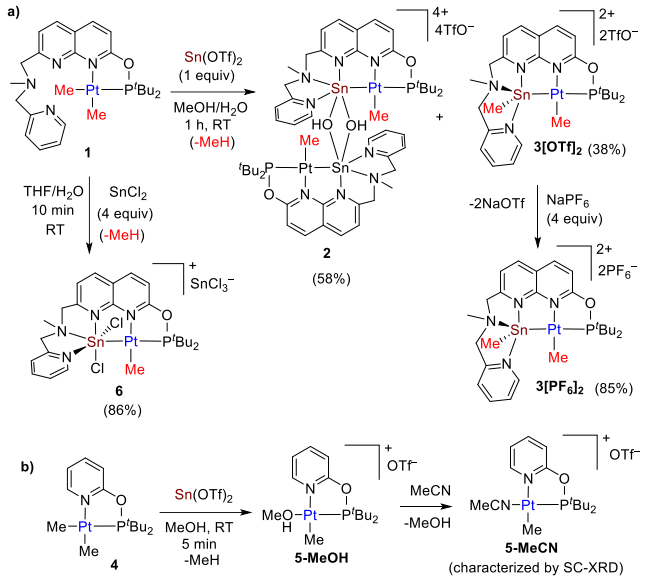

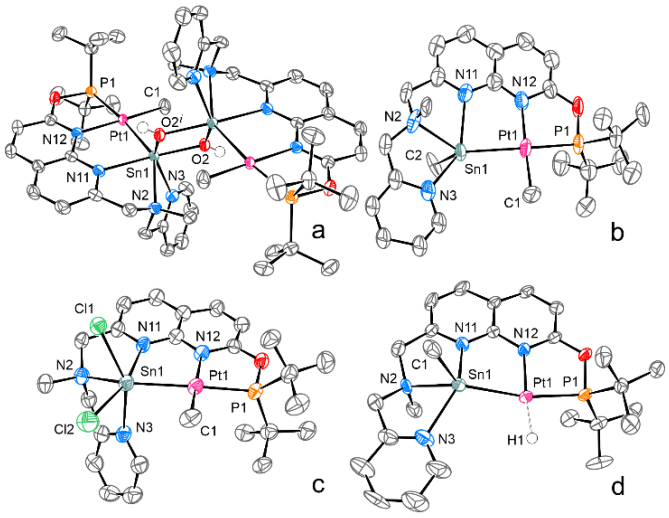

Figure 1. Structures of **2** (a), **3[PF$_6$]$_2$** (b), **6** (c), and **7[PF$_6$]$_2$** (d) in the crystals with thermal ellipsoids at the 80% (a) and 50% (b-d) probability levels. All hydrogen atoms except for [O]H in **2** and [Pt]H in **7[PF$_6$]$_2$**, co-crystallized solvent molecules, disorder components, and counterions are omitted for clarity. Symmetry code *i*: 2–*x*, –*y*, 1–*z*.

Single crystal X-ray crystallography (SC-XRD) of **2** revealed two symmetrical L-PtSn moieties, bridged by two hydroxide ligands via tin, featuring Sn–O distances of 2.1012(13) and 2.1419(15) Å (Figure 1a). The OH groups appear as a singlet at 6.59 ppm in ^{1}H NMR spectrum. The formation of **2** involves initial protonolysis of one of the PtMe groups with methanol or water, which was confirmed by *in situ* ^{1}H NMR detection of methane formation (CH_3D in the case of MeOH-d_4). While such protonolysis is expected to initially generate Sn methoxide core, only stable hydroxide derivative **2** could be crystallized successfully

despite our attempts to obtain methoxide analog in the absence of added water. Each PtMe center is coordinated to a Sn of an $Sn_2(\mu\text{-}OH)_2$ core characterized by relatively short Pt–Sn interatomic distances (2.56718(14) Å), similar to reported platinum(II) stannylene complexes.[9, 19] Considering coordination to Sn, the coordination sphere of Pt remains close to the ideal square planar (τ_4 = 0.07, τ_4' = 0.05). Interestingly, each Sn atom is surrounded by three N-atoms of the chelating N-donor pocket showing relatively long Sn–N distances in the range of 2.3128(16)-2.3882(16) Å.

Table 1. ^{31}P, ^{195}Pt, and ^{119}Sn NMR chemical shifts and coupling constants for complexes 2, 3[X]$_2$, 6, and 7[X]$_2$ (X = OTf or PF$_6$).

Complex	δ ^{31}P ($^1J_{PPt}$, Hz)	δ ^{195}Pt[a]	δ ^{119}Sn ($^2J_{SnP}$, Hz) or δ ^{29}Sn ($^2J_{SiP}$, Hz)
2[a]	181.6 (3467)	−4440.2	–357.6 (5007)
3[OTf]$_2$[a]	185.6 (3495)	−4283.5	106.8 (3465)
3[PF$_6$]$_2$	186.3 (3494)[a]	–4284.7[a]	124.3 (3400)[b]
6[b]	184.5 (3308)	–4401.0	–235.0 (5492)[c]
7[OTf]$_2$[a]	211.43 (3385)	-4970.3	208.9 (3140)
7[PF$_6$]$_2$[a]	210.8 (3375)	–4971.0	209.7(3011)
8[a]	184.8 (3467)	–4439.5	−333.9 (5032)
9[b]	182.7 (3185)	–4401.0	N/A[d]
10[a]	204.5 (2161)	–4306.3	–21.5 (401)
11[a]	205.3 (2076)	−4308.3	–28.0 (384)

[a] In CD_3CN. [b] In CD_2Cl_2. [c] For Pt–Sn core; –44.0 for $SnCl_3^-$ counter anion. [d] Signal was not observed presumably due to coupling to F and low intensity of a multiplet.

Consistent with SC-XRD structure, only one Me group was detected in ^{1}H and ^{13}C{^{1}H} spectra of isolated **2** present at –31.33 ppm in ^{13}C{^{1}H} NMR spectrum, exhibiting coupling to phosphorus ($^2J_{PC}$ 3.4 Hz) and accompanied by ^{195}Pt satellites ($^1J_{PtC}$ = 605 Hz). The ^{119}Sn{^{1}H} spectrum showed a doublet at –357.6 ppm coupled to the phosphorus atom ($^2J_{SnP}$ = 5007 Hz).

By contrast to **2**, the ^{13}C{^{1}H} NMR spectrum of **3[OTf]$_2$** exhibited signals corresponding to two inequivalent Me groups at –32.9 ppm and 5.95 ppm. While the Me group resonance at –32.9 showed the expected coupling to Pt and P similar to the signal observed in **2** ($^1J_{PtC}$ = 587.8 Hz, $^2J_{PC}$ = 3.5 Hz), the second Me group showed coupling to ^{119}Sn (17.3 Hz) but no coupling to ^{195}Pt. These suggested that one of the Me groups had completely migrated from Pt to Sn. Interestingly, the ^{119}Sn spectrum of **3[OTf]$_2$** also showed a significantly shifted ^{119}Sn resonance at 106.8 ppm. Triflate gave only one signal in the ^{19}F NMR spectrum at –79.30 ppm, corresponding to a free triflate counter anion, and the FT-IR spectrum is consistent with the presence of uncoordinated triflate.[20] Attempts to improve reaction selectivity towards **3**$^+$ and to avoid completing protonolysis that forms **2** by using aprotic and less polar solvents led to worse outcomes.

While single crystals of **3[OTf]$_2$** allowed us to establish the expected structure of the bimetallic SnMe/PtMe core with Pt–Sn interatomic distances of 2.570(3) and 2.581(2) Å for two disorder components, the exact positions for one of the triflate counteranions, as well as CH_2Cl_2 co-crystallized solvent molecule, could not be assigned and required SQUEEZE procedure for the final refinement.[21] To obtain better quality structure, complex **3[OTf]$_2$** was subjected to a counteranion exchange using 4 equiv of $NaPF_6$ to give analogous **3[PF$_6$]$_2$**, which showed almost identical ^{1}H, ^{13}C{^{1}H}, and ^{195}Pt{^{1}H} NMR spectra as **3[OTf]$_2$** and could be fully characterized by SC-XRD allowing to clearly establish the structure of the bimetallic SnMe/PtMe core and confirm the presence of two PF_6 counteranions (Figure 1b). The structure of **3[PF$_6$]$_2$** revealed the Me group migration from Pt to Sn, showing the Pt1–C1 and Sn1–C2 bond lengths of 2.053(12) Å and 2.124(19) Å, respectively, for the main disorder component. Surprisingly, no other anionic ligands are present at the formally cationic Sn^{II}Me center, with Sn coordination supplemented by bonding to Pt (Pt–Sn 2.5776(12) and 2.5894(19) Å) and interactions with three neutral N-donors of the ligand N-pocket showing elongated Sn–N distances (2.289(12)-2.391(10) Å). The Pt center remains four-coordinate, with slightly greater deviation from the square planar geometry (τ^4 = 0.16, τ^4' = 0.10 for the main disorder component) compared to **2**.

Although several resonance structures may contribute to the bimetallic Pt–Sn core and oxidation state assignment is not unambiguous,[9, 15f] complexes **2** and **3[X]$_2$** may be best described as Pt^{II}-stannylene complexes, which is in good agreement with their structural and computational analysis (*vide infra*). The coordination geometry around Pt does not undergo significant change during the formation of **2** and **3[X]$_2$** (X = OTf or PF_6) and remains close to square planar; the ^{195}Pt chemical shift also remains within the range expected for Pt^{II} complexes in a similar ligand environment.[17a, 17c] Thus, complexes **3[X]$_2$** represent rare examples of Pt complexes coordinated to a cationic, ligand-stabilized Me–Sn:$^+$.

Cationic organostannylenes have been previously synthesized by salt metathesis with weakly coordinating anions, or by hydride or methanide abstraction with a Lewis acid.[10d, 10e, 11a] To the best of our knowledge, the formation of cationic alkyl stannylenes derivatives via transmetalation from late organotransition metals have not been previously reported.

Stannylenes **3[X]$_2$** are surprisingly stable, showing no significant changes in MeCN solution at RT for 1-2 weeks, which is in contact with the typically highly reactive nature of cationic stannylenes. Such high stability may be due to the stabilizing effect of the Sn interaction with three nitrogen atoms of the chelating ligand and the stabilization of the bimetallic core using the naphthyridine backbone.

To determine whether the binucleating ligand **L** is a key factor in favoring methyl group transfer by supporting metal–metal interactions, we attempted to react the model Pt^{II} complex **4**, supported by a mononucleating (di-*tert*-butylphosphinito)pyridine ligand with a tin salt. When complex **4** was treated with an equivalent amount of Sn^{II}(OTf)$_2$ under identical conditions in MeOH, Pt–Me protonolysis was observed exclusively after 5 min at RT (Scheme 2b), while no transmetalation occurred. Therefore, despite a lesser contribution of competitive protonolysis to generate **2**, the ability of **L** to support a bimetallic core and the presence of a Lewis-basic N-binding pocket altered the reactivity of a Lewis-acidic tin(II) even in a protic solvent such as

methanol. The experiment also showed that **L** is required to stabilize the Sn–Me bond towards further protonolysis.

We hypothesized that the presence of weakly coordinating triflate was another important factor in inducing facile Me group migration. Indeed, when complex **1** was treated with $Sn^{II}Cl_2$ in wet THF, no transmetalation was observed, and Pt–Me protonolysis became predominant, resulting in complex **6**, which features a neutral dichlorostannylene bound to Pt with Pt–Sn of 2.5758(4) Å and Sn–Cl of 2.4363(18) and 2.5121(14) Å according to SC-XRD (Figure 1c).

Pt-to-Stannylene Me Group Transfer Induced by B–H, Si–H, and H_2 Activation. While facile Me group transfer from the neutral dimethyl Pt^{II} fragment was observed in complexes **3[X]$_2$**, we expected that transmetalation from a formally cationic monomethyl Pt complex should be significantly more challenging, explaining the lack of transmetalation once a stable dihydroxy-bridged complex **2** was obtained. We, therefore, sought to induce its reactivity by removing hydroxo groups using common hydride sources, boranes, or silanes. Previous literature reports indicate that the treatment of Sn^{II} alkoxide with pinacolborane is a convenient method for *in situ* generation of an unstable Sn^{II} hydride;[22] other borohydrides and aluminum hydrides have similarly been utilized for the generation of Sn^{II}–H species.[23] Based on this, we examined the reactivity of **2** with common hydride sources and H_2.

Scheme 3. Me group transfer from Pt to stannylene induced by bimetallic hydride formation from boranes, silanes, and H_2.

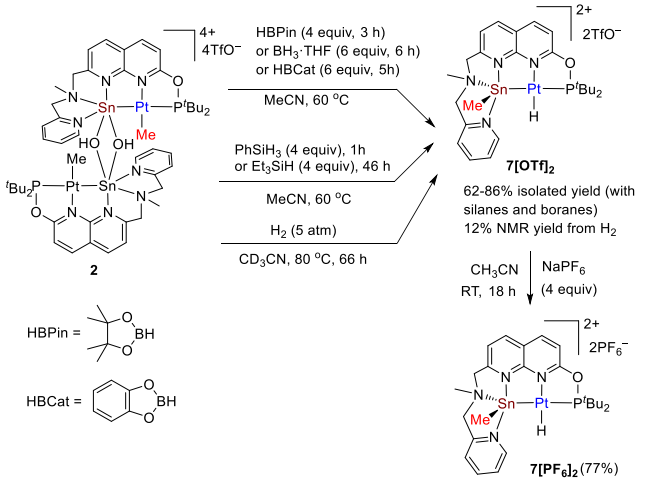

When complex **2** was treated with excess pinacolborane, a slow reaction was observed at RT, which could be accelerated by mild heating at 60 °C for 2 hours to give a new product **7[OTf]$_2$** isolated in 62% yield (Scheme 3). The same complex could be obtained by mild heating of the solution of **2** in the presence of catecholborane or borane THF adduct to give **7[OTf]$_2$** in 67-76% isolated yields. Interestingly, similar but more sluggish and less selective reactivity was observed when **2** was heated at 80 °C under H_2 gas (5 atm) to give **7[OTf]$_2$** in ca. 12% NMR yield (by NMR integration against an internal standard) after 66 hours, along with other unidentified products. A more selective transformation was observed when **2** was treated with $PhSiH_3$ or Et_3SiH to produce **7[OTf]$_2$** in 71-86% isolated yields.

Surprisingly, the ^{1}H NMR spectrum of **7[OTf]$_2$** clearly showed the presence of a hydride peak at –14.64 ppm ($^2J_{PH}$ = 5.2 Hz, $^2J_{SnH}$ = 148 Hz, and $^1J_{PtH}$ = 1125.5 Hz). The ^{119}Sn resonance of **7[OTf]$_2$** appeared at 208.9 ppm characterized by moderate coupling to phosphorus ($^2J_{SnP}$ = 3140 Hz) similar to that seen in **3**.

The X-ray structure of **7[OTf]$_2$** showed a similar cationic bimetallic SnMe/PtH core to **3** with Pt–Sn of 2.6132(13) and 2.6015(13) Å for the disorder components. However, the unit cell contains highly disordered triflate anions, as well as co-crystallized solvent molecules of dichloromethane, which were treated as a diffuse contribution to the overall scattering without specific atom positions by PLATON/SQUEEZE.[21] Complex **7[OTf]$_2$** was subjected to a counteranion exchange with $NaPF_6$ to obtain an analogous complex **7[PF$_6$]$_2$**, which featured almost identical NMR spectra and provided single crystals suitable for SC-XRD analysis. SC-XRD revealed a dicationic Pt(H)−SnMe core with Pt−Sn interatomic distances of 2.5532(12) and 2.529(2) Å for the main and minor disorder components, respectively, and two PF_6^- counter anions (Figure 1d).

We attempted to detect reaction intermediates by monitoring the reaction progress by ^{1}H NMR when **2** was treated with 4 equiv of pinacolborane in CD_3CN solution. Interestingly, two intermediate metal hydride signals were observed, assigned as **Int1** and **Int2**. The new signal corresponding to **Int1** appeared after 5 min at 23 °C in a downfield region at 10.87 ppm showing splitting from tin and phosphorus (J_{HP} = 50.1 Hz, J_{SnH} = 329.2 Hz) (Figure 2). The chemical shift is comparable to those reported for low-valent tin(II) hydrides,[23-24] and a similar signal was observed when complex **2** was treated with phenylsilane and catecholborane. Another intermediate, **Int2**, was characterized by an upfield shifted hydride signal −0.59 ppm showing platinum satellites (J_{HPt} = 947.6 Hz) and larger splitting from phosphorus (J_{HP} = 148.3 Hz) (Figure 2). The latter signal is very similar to the bridging hydride signal observed in bimetallic Zn···H–Pt(Me) complexes supported by the same binucleating ligand and reported earlier.[17c] Signals of both **Int1** and **Int2** diminish in intensity and disappear at longer reaction times.

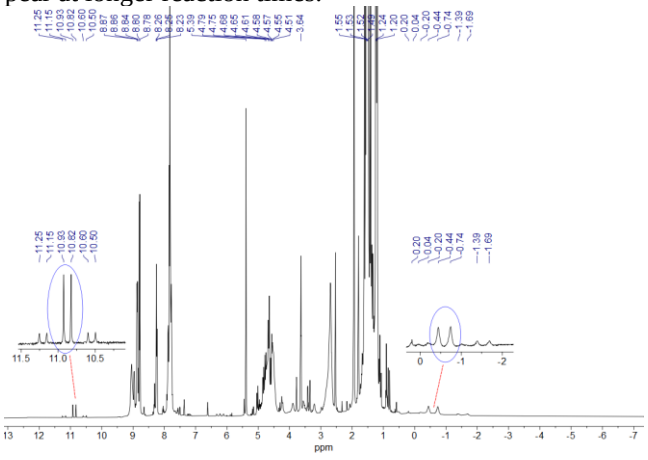

Figure 2. ^{1}H NMR spectrum recorded after treatment of **2** with pinacolborane for 5 min at RT in CD_3CN.

Bimetallic reactivity was required for the observed activation of B–H, Si–H, and H_2 as no Pt–H was formed when a mononuclear complex **1** was treated with boranes, silanes, or H_2 with or without $Sn(OTf)_2$.[17c] The presence of nucleophilic OH groups also plays an important role in borane and silane activation, as dichlorostannylene complex **6** showed no reactivity. The basic properties of $Sn_2(\mu\text{-}OH)_2$ were confirmed by their ability to deprotonate 1,3-diphenyl-1,3,-propanedione to form a cationic stannylene **8** within 5 min at RT in CH_3CN solution (Figure 3a).

Scheme 4. Nucleophilic reactivity of 2.

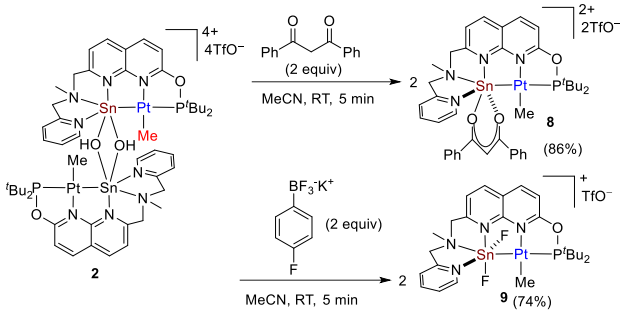

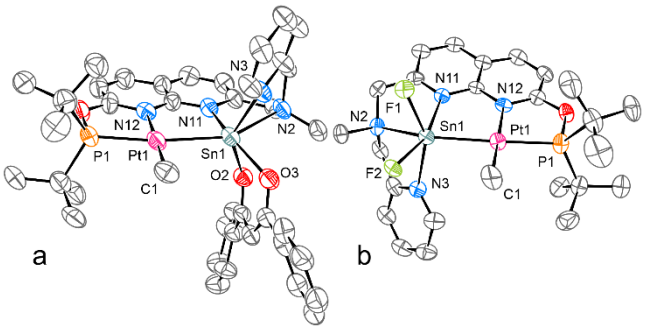

Figure 3. ORTEP of **8** (a) and **9** (b) at the 50% and 60% probability levels, respectively. All hydrogen atoms, co-crystallized solvent molecules, and counterions are omitted for clarity. In the case of **8**, one of two symmetry-independent molecules is shown.

The $Sn_2(\mu\text{-}OH)_2$ core was also reactive in nucleophilic attack at potassium phenyltrifluoroborate to give difluorostannylene **9** that resulted from OH/F exchange (Scheme 4 and Figure 3b). By contrast to dichlorostannylene **6**, difluorostannylene **9** was reactive with pinacolborane to give **7[OTf]$_2$** in 82% NMR yield after 4 hours at 60 °C, suggesting that the presence of nucleophilic ligands (hydroxide or fluoride) at Sn is important for borane activation.

The comparison of $^{119}Sn\{^1H\}$ NMR spectra of all obtained cationic and neutral Pt stannylene complexes (Table 1) shows that cationic methylstannylene complexes **3[X]$_2$** and **7[X]$_2$** are characterized by a significant shift to lower field (106.8-209.7 ppm ppm) as compared to complexes **2**, **6**, and **8** (–235.1 to –357.6 ppm), which is commonly associated with the reduced coordination number at the Sn atom.[11a]

Based on the reported ability of tin(II) alkoxides to react with boranes to give Sn^{II}–H,[22] we proposed that the first step of borane activation by **2** involves the formation of intermediate tin hydride, which is likely accompanied by disassembly of the tetrametallic core to give **Int1**. This is consistent with the observation of the signal of acidic tin hydride at 10.87 ppm with Sn satellites observed by NMR (Figure 2).

We performed DFT calculations to elucidate the mechanism of hydride and Me group transfer leading to the formation of **7**. Calculations were performed using the ωB97XD functional[25] and def2tzvp basis sets[26] for all elements (default ECPs for Pt and Sn). All structures were fully optimized in acetonitrile using the SMD model.[27] Free energies were calculated by frequency calculations at the same level of theory and reported as the sum of solvent-corrected electronic and thermal free energies relative to **Int1**.

From **Int1**, an accessible transition state **TS-H** was identified for the hydride transfer from Sn to Pt to form intermediate **Int2** featuring a bridging hydride, where the hydride mostly resides on the Pt (1.650 Å) and shows a relatively close distance to Sn (Sn–H 2.123 Å) (Scheme 5). This is consistent with the experimentally observed signal at –0.59 ppm (Figure 2; see discussion above), where the chemical shift and coupling constants closely resemble the $(Me)Pt^{II}$–H···Zn core in previously reported bimetallic Pt/Zn complexes supported by an analogous ligand.[17c] Hydride transfer from Sn to Pt and other 2nd and 3rd row TM has also been reported in the literature.[5, 28]

While no transition state could be identified for the direct transfer of the PtMe group present *trans* to N-atom of naphthyridine in **Int2** to form **7**, we hypothesized that the Me group transfer may require initial *cis-trans* isomerization to form **Int3** containing a Me group *trans* to a P-atom and present in closer proximity to Sn. *Cis-trans* isomerization in square-planar complexes is well established and often requires heating at moderate temperatures.[29] The formation of **Int3** is only slightly endergonic, from which a low-barrier process via **TS-Me** results in a Me group transfer to form **7**. Overall, the reaction is driven by the formation of a thermodynamically more stable product **7** featuring a PtH/SnMe core as compared to PtMe/SnH core in **Int1**.

Scheme 5. Proposed mechanism of complex 7 formation by treatment of 2 with boranes.

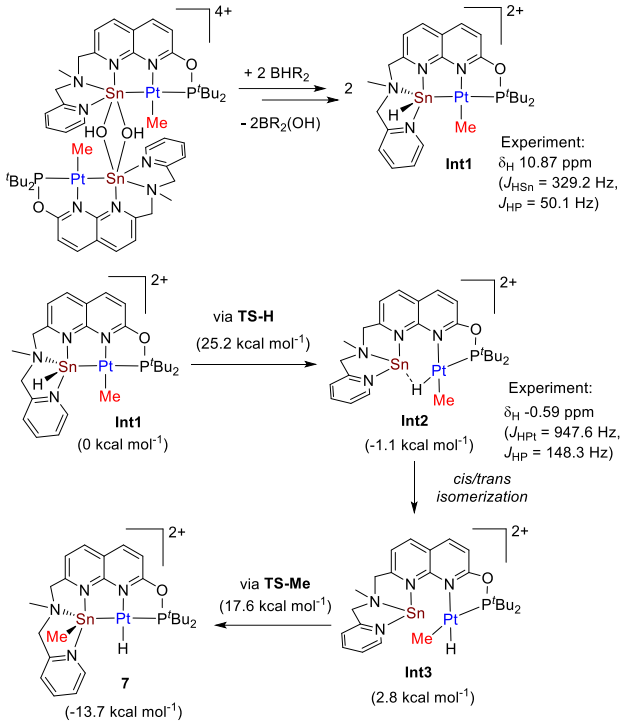

Synthesis of Pt Complexes with Cationic Silylenes. Compared to cationic stannylenes, access to cationic silylenes is complicated due to lower stability of low valent Si^{II} derivatives, although several examples of cationic silylenes have been reported, often supported by amide, iminophosphorane, NHC donors or cyclopentadienyls.[1d, 10a-c, 12b] While neutral silylene complexes are known, transition metal complexes with cationic silylenes are exceedingly rare. For example, Inoue and co-workers reported the reaction of phosphasilene with Pt^0 or Pd^0 precursors to undergo P–Si bond splitting and generate binuclear low-valent Pd–Pd and Pt–Pt complexes with two metals bridged by an amidinate-stabilized Si(II) cation.[14]

In our search for cationic silylene Pt complexes, we found that treatment of Pt precursor **1** with $HSiCl_3$ in the presence of $Zn(OTf)_2$ resulted in the facile and clean formation of complex **10** representing the formal coordination of a Cl–Si:$^+$ to a monomethylplatinum(II) center (Scheme 6). One of the methyl groups likely departs as methane via proton abstraction from trichlorosilane, while Zn is required to remove two chlorides. Complex **10** was isolated in 73% yield and characterized by multinuclear NMR and SC-XRD (Figure 4a).

The facile formation of **10** from $HSiCl_3$ represents an unexpected synthetic route to cationic chlorosilylenes. Using HCl elimination from $HSiCl_3$ has previously been reported as a route to neutral low-valent :$SiCl_2$ and its derivatives; however, this approach requires harsh conditions using phosphonium salts[30] or additives of free NHC to enable the formation of neutral, NHC-stabilized :$SiCl_2$ adducts under mild conditions.[31]

Despite exhaustive attempts, we could not obtain cationic alkylsilylene derivatives from **10** and common alkylating reagents and no stable products were formed. However, chloride could be exchanged by treatment with trimethylsilyl azide (TMS–N_3) to give an analogous stable cationic azidosilylene complex **11**, isolated in 93% yield and characterized by multinuclear NMR and SC-XRD (Scheme 6 and Figure 4b).

Scheme 6. Synthesis of Pt complexes with cationic silylenes.

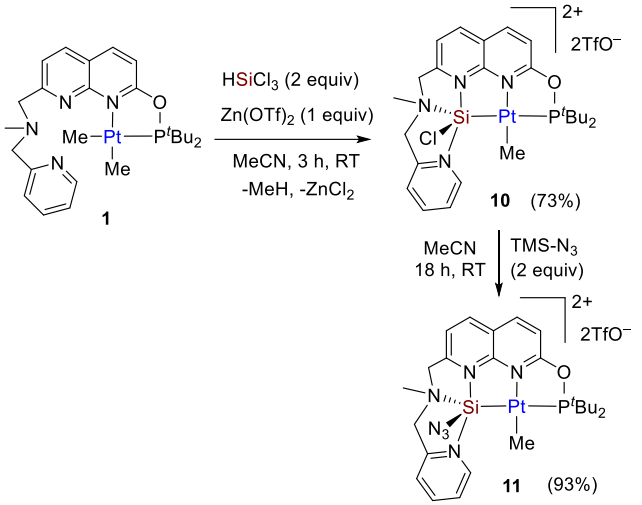

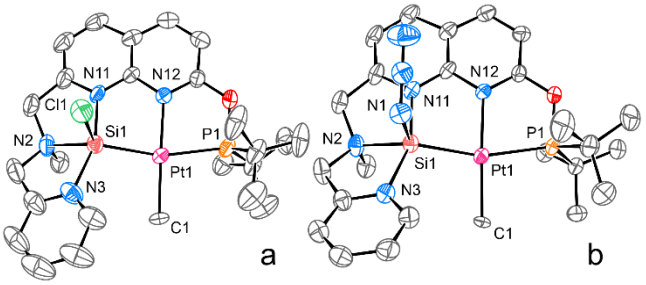

Figure 4. ORTEP of **10** (a) and **11** (b) at the 50% probability level. All hydrogen atoms, co-crystallized solvent molecules, disorder components, and counterions are omitted for clarity.

The Pt–Si distances in **10** and **11** are 2.3200(15) and 2.3291(12) Å, respectively, which is in a range expected for a Pt–Si single bond, but longer compared to complexes where double bond Pt=Si character is reported.[32] Compared to low valent Pt complexes with neutral amidate-supported silylenes and bridging silylene in Inoue's complex,[14] these bonds are also elongated, consistent with mostly single Pt–Si bond character and lack of significant back-donation from Pt. The Si–N distances are in the range of 1.947(5)-1.987(5) Å for **10** and 1.956(4)-2.001(4) Å (Si–N_3 is 1.771(4) Å) for **11**, notably longer than Si–N bonds reported in cationic iminophosphorane or β-diketiminato ligands,[10a-c] which could be attributed to weaker dative interactions with neutral N-heterocycle or tertiary amine donors in ligand **L** (see computational analysis below).

The ^{29}Si resonances of **10** and **11** appear at −21.5 and −28.0 ppm, respectively, showing coupling to phosphorus (401 and 384 Hz, respectively). These chemical shifts resemble signals of free cationic iodo- or chlorosilylenes stabilized by NHC or iminophosphorane donors (−3.3 to −89.9 ppm); however, they differ significantly from the bridging silylene in Inoue's binuclear low-valent Pt–Pt complex (187.8 ppm), presumably due to a different binding mode, ligand environment, and platinum oxidation state. The ^{195}Pt chemical shifts of **10** and **11** are similar to those observed in cationic stannylene complexes (Table 1),

showing no significant changes in electronic character at the Pt center.

Overall, we demonstrate that the binucleating ligand **L** allows facile synthetic access not only to cationic stannylene complexes but also to the much less common N-donor stabilized cationic chlorosilylene complexes, which can be isolated and characterized.

Computational Analysis of Pt–Sn and Pt–Si Bonding. To shed light on the nature of Pt–E (E = Si or Sn) bonding in our complexes featuring cationic stannylene Me–Sn:$^+$ and silylene X–Si:$^+$ (X = Cl or N_3) ligands, we performed quantum theory of atoms in molecules (QTAIM)[33] and natural bond orbital (NBO)[34] analysis of geometry-optimized structures of free cationic complexes **3**, **7**, **10** and **11**.

Coordination of more commonly encountered neutral, :EX_2-type silylenes and stannylenes to a transition metal center is usually described as a donation from a lone pair on a Group 14 element to a TM, which may further be complemented by π-back donation from a TM-based *d*-orbital of a suitable symmetry to a *p*-orbital on the Si or Sn atom. In addition, stannylenes may accept donation from Lewis bases perpendicular to the :EX_2 plane.[2, 15b, 35] Two models of hybridization are usually considered, which are expected to show different angles between substituents at Group 14 elements: sp^2 hybridization (commonly found in carbenes) resulting in a 120° angle between substituents, and an unhybridized model with angles close to 90° as is typical for heavier elements such as tin.[2]

As expected, bond critical points (*bcp*'s) were located between Pt and Sn or Si atoms in all complexes (Figures 5 and S125-S132). The selected characteristics of the *bcp*'s, including the electron density (ρ_b), the Laplacian of the electron density ($\nabla^2\rho_b$), as well as delocalization indices (*DI*, the average number of electrons shared between a pair of atoms), are shown in Table 2 for complexes **3**, **7**, **10**, and **11**. The delocalization indices are in the range of 0.84–0.95, indicative of single bond character. The *bcp*'s corresponding to Pt–E (E = Sn or Si) bonds are characterized by negative values for the total electronic energy density H_b typical for coordination bonds.[36] Coordination of Sn or Si to all three neutral N-donors of the chelating ligand fragment was also confirmed by locating *bcp*'s between Sn or Si and all N-atoms, although these bonds were characterized by significantly smaller delocalization indices (*DI* for Sn–N bonds in the range of 0.29-0.40 for **3** and **7** and 0.25-0.32 for Si–N bonds in **10** and **11**) (Tables S1-S2, S7-S8), suggesting partial bond character and consistent with NBO analysis (*vide infra*). Sn–N and Si–N bonds are characterized by positive $\nabla^2\rho_b$ and negative values for H_b (see ESI).

The Pt–Sn bonds are characterized by the positive value of the Laplacian of the electron density at the *bcp*; at the same time, the *bcp*'s of the Pt–Si bonds are characterized by small negative $\nabla^2\rho_b$. While the positive values of $\nabla^2\rho_b$ have been commonly interpreted in terms of closed-shell interactions and negative values have been associated with the "shared" interactions,[37] the interpretation of these values is less conclusive when bonding involving heavy elements is considered and the positive values may reflect bonding to a heavier Sn, as compared to Si.[36b] The ratios of the absolute electronic potential energy to kinetic energy densities at the *bcp*'s, $|V_b|/G_b$, is between 1 and 2 for stannylenes **3** and **7**, typical for intermediate bonds and greater than 2 for **10** and **11**, which may reflect greater covalency of Pt–Si bonding in silylenes.[36a, 37a, 38]

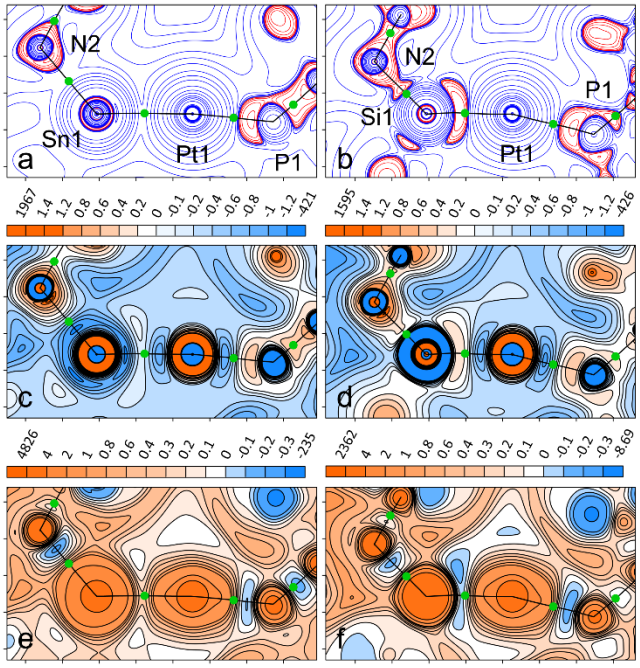

Figure 5. Contour maps of $\nabla^2\rho(\mathbf{r})$ (a, b), $\varphi_W(\mathbf{r})$ (c, d), and $\varphi_f(\mathbf{r})$ (e, f) calculated for cationic complexes **3** (a, c, e) and **10** (b, d, f) and plotted on atomic planes of E1 (E = Sn or Si), Pt1, and N2. For the $\nabla^2\rho(\mathbf{r})$-maps, the logarithmic scale is adopted in the form of ± 2, 4, $8\cdot10^n$ ($-3 \le n \le 2$) a.u. Scale bars of the potential function (in a.u.) are displayed above the plots. The distance between adjacent axis tick marks is 1 Å. Bond critical points and bond paths are indicated by green dots and black lines.

The analysis of the scalar fields $\nabla^2\rho(\mathbf{r})$, $\varphi_W(\mathbf{r})$, and $\varphi_f(\mathbf{r})$ can provide substantial information about the subatomic structure of the metals Pt and Sn and the metalloid Si, involved in the bonds Pt–Sn and Pt–Si. The Laplacian of the electron density $\nabla^2\rho(\mathbf{r})$, which is widely used to characterize the curvature of the electron density, highlights that in regions where $\nabla^2\rho(\mathbf{r}) < 0$, the potential energy makes a dominant contribution to the total electronic energy of a system.[38b, 39] The von Weizsäcker potential $\varphi_W(\mathbf{r})$, also known as the bosonic kinetic potential, identifies classically allowed ($\varphi_W(\mathbf{r}) > 0$) and forbidden ($\varphi_W(\mathbf{r}) < 0$) regions for electrons, and can distinguish between core- or valence-shell charge concentrations and depletions, respectively.[40] Furthermore, the fermionic potential $\varphi_f(\mathbf{r})$, which indicates regions where the static exchange correlation ($\varphi_f(\mathbf{r}) < 0$) or kinetic exchange correlation ($\varphi_f(\mathbf{r}) > 0$) dominates, can identify electron pairs.[41] Notably, both $\varphi_W(\mathbf{r})$ and $\varphi_f(\mathbf{r})$ reveal the electron localization and the explicit arrangement of depleted regions around cationic metals.[41a]

Table 2. Selected bond critical point (*bcp*) properties for Pt–E (E = Sn or Si) bonds in geometry-optimized[a] complexes 3, 7 (E = Sn), 10, and 11 (E = Si) and interatomic Pt–E distances (*d*, Å) from SC-XRD.

Complex	ρ_b [b]	$\nabla^2\rho_b$ [c]	H_b [d]	$\lvert V_b\rvert/G_b$ [e]	*DI* [f]	*d* [g]
3	0.073965	0.056238	-0.025906	1.648	0.845164	2.5776(12)[h]
7	0.077543	0.057573	-0.028243	1.662	0.895016	2.5532(12)[i]
10	0.105922	-0.07495	-0.058014	2.477	0.949863	2.3200(15)
11	0.105222	-0.07516	-0.057051	2.491	0.942575	2.3291(12)

[a] At ωB97XD/def2tzvp level, see SI for details. [b] Electron density (a.u.). [c] Laplacian of electron density (a.u.). [d] The total energy density density (a.u.). [e] Ratio between the absolute electronic potential energy and kinetic energy densities. [f] Delocalization index. [g] Interatomic distance (Å) from SC-XRD. [h] For the main disorder component of **3[PF$_6$]$_2$**. [i] For the main disorder component of **7[PF$_6$]$_2$**.

Figure 5 shows contour maps of the abovementioned functions plotted on the plane containing E1 (E = Sn or Si), Pt1, and N2 of the optimized cationic complexes **3** and **10**; note that the nuclei P1 are off the map planes. The coordination bonds Pt1–P1 illustrate a donor–acceptor bonding mechanism. For each complex (Figure 5, c and d), P1 exhibits a well-shaped valence-shell charge concentration (VSCC) ($\varphi_W(\mathbf{r}) > 0$) directed along the internuclear line Pt1–P1 to a pronounced outer-shell depletion at Pt1 ($\varphi_W(\mathbf{r}) < 0$). The former can be confidently assigned to an electron pair, since it corresponds to a region with $\varphi_f(\mathbf{r}) < 0$, while the latter can be associated with a vacancy ($\varphi_f(\mathbf{r}) > 0$). A comparable situation is observed for the coordination bond Sn1–N2 in **3**, where the nitrogen and tin atoms play the role of a Lewis base and a Lewis acid, respectively. However, judging from the maps, the bond Si1–N2 in **10** is characterized by a more elongated VSCC (Figure 5d), as well as a negative curvature of the electron density (Figure 5b), in the middle of the internuclear line and simultaneously shows a shift of the electron pair localization region toward the bond center (Figure 5f), compared to that in **3**. This suggests that the bond Si1–N2 is strongly polar covalent in nature.

The behavior of the two sets of functions for the bonds Pt–Si and Pt–Sn differ as well. As shown in Figure 5, d and f, the apparent electron pair and vacancy in the outer shells of Si1 and Pt1, respectively, lie along the bond path, and thus the coordination bond Pt1–Si1 in **10** has a pronounced donor–acceptor character. At the same time, a vacancy can be observed for each metal atom along the bond path Pt1–Sn1 (Figure 5c). Highly positive values of $\varphi_f(\mathbf{r})$ along the bond path suggest the absence of the electron pair localization region along the heteronuclear metal bond Pt–Sn (Figure 5e). In the wide central zone between the atoms Pt1 and Sn1, the signs of the functions do not change, while their values indicate a scarcity of electrons. Although such behavior is common in other bimetallic systems combining two heavy elements,[38c, 42] this indicates the differences in the character of Pt–Si vs. Pt–Sn bonding, which prompted ups to further investigated Pt–Si and Pt–Sn bonding by NBO analysis.

The natural localized molecular orbitals (NLMO) were identified for complexes **10** and **11** that correspond to Pt–Si bonding. In the case of complex **10**, the NLMO contributing to Pt–Si bonding is comprised of the *sd* hybrid on Pt (37% from parent NBO on Pt; with individual atomic hybrid contributions of *s* 40% and *d* 60%) and an *sp*-hybrid orbital of Si (60% from the parent NBO on Si; *s* 60%/*p* 40%), with a minor contribution from a carbon of Pt–Me (1%) (Figure 6b). The NLMO associated with Pt–Si bonding in **11** has a similar composition (38% Pt, 59% Si) (Figure S145).

The NLMO contributing to a notably less pronounced Pt–Sn bonding (Pt–Sn LMO bond order 0.28 as compared to Pt–Si LMO order of 0.74 in **10**) largely has the character of a lone pair residing at Sn (76%) (Figure 6a) with less significant contribution from the *sd*-hybrid orbital at Pt (14%) and the *sp*-hybrid orbital at the phosphorus (7%). Similarly, the NLMO contributing to Pt–Sn bonding in **7** has largely the character of the lone pair at Sn (75% Sn, 15% Pt, and 8% P) (Figure S139). In both complexes **3** and **7**, the lone pair at Sn has a significant *s*-character (*s* 77%/*p* 23% in **3**; *s* 76%/*p* 24% in **7**) as expected from heavy Group 14 elements when compared to Si or carbon.

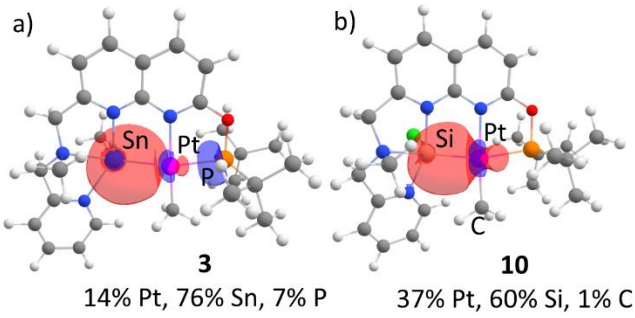

Figure 6. NLMO's contributing to Pt–Sn or Pt–Si bonding in complexes **3** (a) and **10** (b).

The second-order perturbation analysis of donor-acceptor interactions in complex **3** shows a significant donation from a lone pair on Sn to an antibonding σ*(Pt–P) orbital and an antibonding σ*(Pt–C) orbital ($E^{(2)}$ = 336.9 and 97.7 kcal mol^{-1}, respectively) (Table S9). Backdonation from Pt-based *d*-orbital to an empty *p*-orbital on Sn is relatively weak ($E^{(2)}$ = 16.0 kcal mol^{-1}), as expected for stannylenes stabilized by Lewis bases, in this case, N-donors of picolylamine chelating pocket. A similar bonding situation is present in complex **7** with main donor–acceptor interactions between Pt and Sn involving the donation from a lone pair on Sn to a σ*(Pt–P) and σ*(Pt–H) ($E^{(2)}$ = 372.8 and 89.6 kcal mol^{-1}) with only a minor backdonation from Pt *d*-orbital to an empty *p*-orbital of Sn ($E^{(2)}$ = 11.5 kcal mol^{-1}) (Table S12).

For comparison, the Pt–Si bonding is not described in terms of donor-acceptor interactions in complexes **10** and **11** showing one bonding NBO localized between Pt and Si

(Figure 6b), which could be due to its more covalent character and stronger Pt–Si bonding.[38c]

The comparison of Wiberg bond indices and delocalization indices shows significantly higher Pt–Si bond orders in **10** and **11** close to single bonds and reduced bond order for Pt-Sn bonds in **3** and **7** (Tables 2-3).

The predominant *s*-character of the Sn-based lone pair in methylstannylenes **3** and **7** is also consistent with H_3C−Sn−N(Me) angles that are close to 90° both in SC-XRD and in geometry-optimized structures (93.5(7) and 93.6(3)° from SC-XRD for the main disorder components of **3[PF$_6$]$_2$** and **7[PF$_6$]$_2$**; 93.7° and 93.4° in geometry-optimized **3** and **7**, respectively) (Table S21). Contribution from *d*-orbitals on Sn was negligible in all cases (<0.5%) and was not necessary to describe the bonding in accordance with the literature reports. Consistent with expectedly more pronounced *sp*-hybridization in the case Si compared to Sn, the X–Si–N(Me) (X = Cl or N-atom of azide) angles show greater deviation from 90° (105.66(17)° and 104.68(19)° from SC-XRD for **10** and **11**; 102.3° and 101.0° in geometry-optimized **10** and **11**, respectively) (Table S21). The comparison of Wiberg bond indices (WBI) correlates with experimental and computed Pt−Sn bond distances showing larger WBI's corresponding to shorter Pt−Sn distances, e.g., in complex **7** compared to **3** (Table 3 and S21).

In all cases, the donation from the N-atom of the heterocycles and tertiary amine to Sn or Si is characterized by Wiberg bond indices values that are significantly smaller than expected from a single bond suggesting partial bond character and consistent with relatively long bond distances.

Table 3. Wiberg bond indices (WBI) for selected bonds in geometry-optimized 3, 7, 10, and 11.[a]

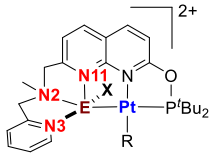

3: E = Sn, X = Me, R = Me
7: E = Sn, X = Me, R = H
10: E = Si, X = Cl, R = Me
11: E = Si, X = N_3, R = Me

Complex	Pt−E	E−X	E−N2[b]	E−N11[c]	E−N3[d]
3 (E = Sn)	0.444	0.777	0.249	0.232	0.296
7 (E = Sn)	0.467	0.785	0.250	0.228	0.304
10 (E = Si)	0.569	0.839	0.339	0.314	0.369
11 (E = Si)	0.571	0.637	0.344	0.302	0.381

[a] At ωB97XD/def2tzvp level, see SI for details. [b] Si/Sn bond with N-atom of tertiary amine (see scheme above for N-atom numbering). [c] Si/Sn bond with N-atom of naphthyridine. [d] Si/Sn bond with N-atom of pyridine.

To summarize, QTAIM analysis indicates that although Pt–Sn and Pt–Si bonding is present in all complexes, real space function and NBO analyses reflect differences in the bond character showing generally higher bond orders for Pt–Si bonds and the well-pronounced donor–acceptor character of Pt–Si bonds according to a detailed analysis of electronic potentials, as well as the Laplacian of the electron density. At the same time, Pt–Sn bonding in cationic methylstannylene complexes **3** and **7** is described in NBO analysis as the donation from the *s*-character lone pair at Sn to a Pt-containing fragments, which reflects that the coordination properties of the methylstannylene motif are determined by donation from the lone pair of Sn.

Although Sn and Si centers still possess an empty orbital that accepts donation from all three N-donors of the ligand, these interactions show partial bonding character, resulting in elongated bonds and are consistent with diminished bond indices (WBI and DI). Therefore, while N-donors are important for stabilization of these unusual cationic stannylene and silylene complexes, these interactions are expected to be significantly weaker as compared to anionic ligands typically used to stabilize cationic silylenes and stannylenes. This could be due to the neutral character of N-heterocycle or tertiary amine donors, or due to the geometric constraints imposed by the binucleating ligand.

Conclusion

In summary, we have developed a new family of stable cationic methylstannylene and cationic silylene complexes with Pt(II). Methylstannylenes were obtained by facile methyl group migration from either dimethyl or a monomethyl Pt; in the latter case, the Me group transfer is triggered by activation of B–H, Si–H, and H–H bonds and concomitant hydride transfer from Sn to Pt, as confirmed by Sn–H intermediates observed via NMR. To the best of our knowledge, this is the first report on the use of methyl group transfer for the synthesis of cationic alkylstannylenes in complexes with transition metals. The computational study presented in this work provided insight into the character of Pt-tetrel bonding in cationic stannylenes and silylenes and the role of weak coordination of neutral N-donors in stabilizing cationic tetrel fragments.

Such an approach can be further exploited for the design of new reactive TM/tetrel metal complexes in which the Lewis acidic character is still retained at the cationic Sn or Si centers. Here, binucleating ligand stabilization likely played an important role in the experimentally observed facile transmetalation from dimethyl Pt complex to Sn^{2+} in the presence of weakly coordinating anions. Future studies will be directed towards the utilization of such systems for selective bimetallic bond activation and alkyl group transfer processes, especially considering the potential application of Pt complexes in C–H bond activation and stability of alkylstannylenes towards hydrolysis.

Supporting Information. Deposition numbers 2253415-2253417, 2263473-2263475, and 2280533-2280537 contain the supplementary crystallographic data for this paper. These data are provided free of charge by the joint Cambridge Crystallographic Data Centre and Fachinformationszentrum Karlsruhe Access Structures service www.ccdc.cam.ac.uk/structures. Synthetic procedures, characterization, and computational details (PDF), Cartesian coordinates (XYZ) for geometry-optimized structures are available in the Supporting Information.

ACKNOWLEDGMENT

The authors thank the Instrumental Analysis section and Engineering section for technical support, the HPC facility for access to computational resources and OIST for funding. R. R. F. acknowledges the support of the Russian Science Foundation (grant No. 21-73-10191) in part of crystal structure determination and the analysis of the scalar fields.

REFERENCES

1. a) Fischer, R. C.; Power, P. P. π-Bonding and the Lone Pair Effect in Multiple Bonds Involving Heavier Main Group Elements: Developments in the New Millennium. *Chem. Rev.* **2010,** *110*, 3877-3923; b) Power, P. P. Main-group elements as transition metals. *Nature* **2010,** *463*, 171-177; c) Hadlington, T. J.; Driess, M.; Jones, C. Low-valent group 14 element hydride chemistry: towards catalysis. *Chem. Soc. Rev.* **2018,** *47*, 4176-4197; d) Swamy, V. S. V. S. N.; Pal, S.; Khan, S.; Sen, S. S. Cations and dications of heavier group 14 elements in low oxidation states. *Dalton Trans.* **2015,** *44*, 12903-12923; e) Shan, C.; Yao, S.; Driess, M. Where silylene–silicon centres matter in the activation of small molecules. *Chem. Soc. Rev.* **2020,** *49*, 6733-6754; f) Okazaki, M.; Tobita, H.; Ogino, H. Reactivity of silylene complexes. *Dalton Trans.* **2003**, 493-506.

2. Agustin, D.; Ehses, M. 119Sn NMR spectroscopic and structural properties of transition metal complexes with terminal stannylene ligands. *C. R. Chim.* **2009,** *12*, 1189-1227.

3. Somerville, R. J.; Campos, J. Cooperativity in Transition Metal Tetrylene Complexes. *Eur. J. Inorg. Chem.* **2021,** *2021*, 3488-3498.

4. a) Handford, R. C.; Nesbit, M. A.; Smith, P. W.; Britt, R. D.; Tilley, T. D. Versatile Fe–Sn Bonding Interactions in a Metallostannylene System: Multiple Bonding and C–H Bond Activation. *J. Am. Chem. Soc.* **2022,** *144*, 358-367; b) Keil, P. M.; Soyemi, A.; Weisser, K.; Szilvási, T.; Limberg, C.; Hadlington, T. J. Cationic Tetrylene-Iron(0) Complexes: Access Points for Cooperative, Reversible Bond Activation and Open-Shell Iron(−I) Ferrato-Tetrylenes**. *Angew. Chem. Int. Ed.* **2023,** *62*, e202218141; c) Widemann, M.; Eichele, K.; Schubert, H.; Sindlinger, C. P.; Klenner, S.; Pöttgen, R.; Wesemann, L. Synthesis and Hydrogenation of Heavy Homologues of Rhodium Carbynes: [(Me3P)2(Ph3P)Rh≡E-Ar*] (E=Sn, Pb). *Angew. Chem. Int. Ed.* **2021,** *60*, 5882-5889.

5. a) Liu, H.-J.; Guihaumé, J.; Davin, T.; Raynaud, C.; Eisenstein, O.; Tilley, T. D. 1,2-Hydrogen Migration to a Saturated Ruthenium Complex via Reversal of Electronic Properties for Tin in a Stannylene-to-Metallostannylene Conversion. *J. Am. Chem. Soc.* **2014,** *136*, 13991-13994; b) Hayes, P. G.; Gribble, C. W.; Waterman, R.; Tilley, T. D. A Hydrogen-Substituted Osmium Stannylene Complex: Isomerization to a Metallostannylene Complex via an Unusual α-Hydrogen Migration from Tin to Osmium. *J. Am. Chem. Soc.* **2009,** *131*, 4606-4607.

6. a) Rankin, M. A.; MacLean, D. F.; Schatte, G.; McDonald, R.; Stradiotto, M. Silylene Extrusion from Organosilanes via Double Geminal Si−H Bond Activation by a Cp*Ru(κ2-P,N)+ Complex: Observation of a Key Stoichiometric Step in the Glaser−Tilley Alkene Hydrosilylation Mechanism. *J. Am. Chem. Soc.* **2007,** *129*, 15855-15864; b) Glaser, P. B.; Tilley, T. D. Catalytic Hydrosilylation of Alkenes by a Ruthenium Silylene Complex. Evidence for a New Hydrosilylation Mechanism. *J. Am. Chem. Soc.* **2003,** *125*, 13640-13641.

7. a) Dias, R. P.; Rocha, W. R. DFT Study of the Homogeneous Hydroformylation of Propene Promoted by a Heterobimetallic Pt–Sn Catalyst. *Organometallics* **2011,** *30*, 4257-4268; b) van Duren, R.; van der Vlugt, J. I.; Kooijman, H.; Spek, A. L.; Vogt, D. Platinum-catalyzed hydroformylation of terminal and internal octenes. *Dalton Trans.* **2007**, 1053-1059; c) Tayim, H. A.; Bailar, J. C. Homogeneous catalysis in the reactions of olefinic substances. VIII. Isomerization of 1,5-cyclooctadiene with dichlorobis(triphenylphosphine)platinum(II). *J. Am. Chem. Soc.* **1967,** *89*, 3420-3424; d) Hsu, C.-Y.; Orchin, M. Hydridotrichlorostannatocarbonylbis(triphenylphosphine)platinum(II) , PtH(SnCl3)(CO)(PPh3)2, as a selective hydroformylation catalyst. *J. Am. Chem. Soc.* **1975,** *97*, 3553-3553.

8. a) Jung, I. G.; Seo, J.; Lee, S. I.; Choi, S. Y.; Chung, Y. K. Reductive Cyclization of Diynes and Enynes Catalyzed by Allyl Platinum N-Heterocyclic Carbene Complexes. *Organometallics* **2006,** *25*, 4240-4242; b) Jang, M.-S.; Wang, X.; Jang, W.-Y.; Jang, H.-Y. Pt(II)/SnX2 (X = Cl, Br)-Catalyzed Cyclization: Completely Different Reactivity of the Platinum Complex toward 1,6-Haloenynes and 1,6-Enynes. *Organometallics* **2009,** *28*, 4841-4844; c) Shinde, M. P.; Wang, X.; Kang, E. J.; Jang, H.-Y. Platinum-Catalyzed Hydrogenative Cyclization of Yne-Enones, Yne-Aldehydes, and Yne-Dienes. *Eur. J. Org. Chem.* **2009,** *2009*, 6091-6094; d) Yoon, H.-S.; Kim, J.-H.; Kang, E. J.; Jang, H.-Y. Platinum-Catalyzed Cyclization of N-Allyl Carbamates for the Synthesis of 5-Vinyloxazolidinones. *Eur. J. Org. Chem.* **2012,** *2012*, 1901-1905; e) Lee, H.; Jang, M.-S.; Hong, J.-T.; Jang, H.-Y. Platinum-catalyzed reductive coupling of activated alkenes under hydrogenation conditions. *Tetrahedron Lett.* **2008,** *49*, 5785-5788.

9. Warsink, S.; Derrah, E. J.; Boon, C. A.; Cabon, Y.; de Pater, J. J. M.; Lutz, M.; Klein Gebbink, R. J. M.; Deelman, B.-J. Intramolecularly Stabilised Group 10 Metal Stannyl and Stannylene Complexes: Multi-pathway Synthesis and Observation of Platinum-to-Tin Alkyl Transfer. *Chem. Eur. J.* **2015,** *21*, 1765-1779.

10. a) Xiong, Y.; Yao, S.; Inoue, S.; Irran, E.; Driess, M. The Elusive Silyliumylidene [ClSi:]+ and Silathionium [ClSiS]+ Cations Stabilized by Bis(Iminophosphorane) Chelate Ligand. *Angew. Chem. Int. Ed.* **2012,** *51*, 10074-10077; b) Driess, M.; Yao, S.; Brym, M.; van Wüllen, C. Low-Valent Silicon Cations with Two-Coordinate Silicon and Aromatic Character. *Angew. Chem. Int. Ed.* **2006,** *45*, 6730-6733; c) Do, D. C. H.; Protchenko, A. V.; Fuentes, M. Á.; Hicks, J.; Vasko, P.; Aldridge, S. N–H cleavage vs. Werner complex formation: reactivity of cationic group 14 tetrelenes towards amines. *Chem. Commun.* **2020,** *56*, 4684-4687; d) Taylor, M. J.; Saunders, A. J.; Coles, M. P.; Fulton, J. R. Low-Coordinate Tin and Lead Cations. *Organometallics* **2011,** *30*, 1334-1339; e) Hino, S.; Brynda, M.; Phillips, A. D.; Power, P. P. Synthesis and Characterization of a Quasi-One-Coordinate Lead Cation. *Angew. Chem. Int. Ed.* **2004,** *43*, 2655-2658; f) Wagner, M.; Zöller, T.; Hiller, W.; Prosenc, M. H.; Jurkschat, K. [4-tBu-2,6-{P(O)(OiPr)2}2C6H2SnL]+: An NHC-Stabilized Organotin(II) Cation and Related Derivatives. *Chem. Eur. J.* **2013,** *19*, 9463-9467; g) Singh, A. P.; Roesky, H. W.; Carl, E.; Stalke, D.; Demers, J.-P.; Lange, A. Lewis Base Mediated Autoionization of GeCl2 and SnCl2. *J. Am. Chem. Soc.* **2012,** *134*, 4998-5003; h) Arii, H.; Matsuo, M.; Nakadate, F.; Mochida, K.; Kawashima, T. Coordination of a chiral tin(ii) cation bearing a bis(oxazoline) ligand with tetrahydrofuran derivatives. *Dalton Trans.* **2012,** *41*, 11195-11200.

11. a) Sindlinger, C. P.; Aicher, F. S. W.; Wesemann, L. Cationic Stannylenes: In Situ Generation and NMR Spectroscopic Characterization. *Inorg. Chem.* **2017,** *56*, 548-560; b) Tanaka, H.; Ichinohe, M.; Sekiguchi, A. An Isolable NHC-Stabilized Silylene Radical Cation: Synthesis and Structural Characterization. *J. Am. Chem. Soc.* **2012,** *134*, 5540-5543.

12. a) Objartel, I.; Ott, H.; Stalke, D. Low-Temperature NMR and Crystal Structure Analyses of a Hemilabile Tin Complex. *Z. Anorg. Allg. Chem.* **2008,** *634*, 2373-2379; b) Yeong, H.-X.; Xi, H.-W.; Li, Y.; Lim, K. H.; So, C.-W. A Silyliumylidene Cation Stabilized by an Amidinate Ligand and 4-Dimethylaminopyridine. *Chem. Eur. J.* **2013,** *19*, 11786-11790.

13. a) Jutzi, P.; Mix, A.; Rummel, B.; Schoeller, W. W.; Neumann, B.; Stammler, H.-G. The (Me5C5)Si+ Cation: A Stable Derivative of HSi+. *Science* **2004,** *305*, 849-851; b) Rhodes, B.; Chien, J. C. W.; Rausch, M. D. (η5-Pentamethylcyclopentadienyl)tin(II) Tetrakis(pentafluorophenyl)borate: A New Cocatalyst for the Polymerization of α-Olefins. *Organometallics* **1998,** *17*, 1931-1933; cJutzi, P.; Kohl, F.; Krüger, C. Synthesis and Structure of the nido-Cluster (CH3)5C5Sn+. *Angew. Chem. Int. Ed.* **1979,** *18*, 59-60.

14. Breit, N. C.; Szilvási, T.; Suzuki, T.; Gallego, D.; Inoue, S. From a Zwitterionic Phosphasilene to Base Stabilized Silyliumylidene-Phosphide and Bis(silylene) Complexes. *J. Am. Chem. Soc.* **2013,** *135*, 17958-17968.

15. a) Keil, P. M.; Hadlington, T. J. Accessing cationic tetrylene-nickel(0) systems featuring donor–acceptor E–Ni triple bonds (E = Ge, Sn). *Chem. Commun.* **2022,** *58*, 3011-3014; b) Jambor, R.; Kašná, B.; Koller, S. G.; Strohmann, C.; Schürmann, M.; Jurkschat, K. [{2,6-(Me2NCH2)2C6H3(H2O)Sn}W(CO)5]+-CB11H12−: Aqua Complex of a Transition-Metal-Bound Organotin(II) Cation versus an Ammonium-Type Structure. *Eur. J. Inorg. Chem.* **2010,** *2010*, 902-908; c) Dostálová, R.; Dostál, L.; Růžička, A.; Jambor, R. Chromiumpentacarbonyl-Coordinated Organotin(II) Cation. *Organometallics* **2011,** *30*, 2405-2410; d) Wagner, M.; Henn, M.; Dietz, C.; Schürmann, M.; Prosenc, M. H.; Jurkschat, K. Chromium Pentacarbonyl-Substituted Organotin(II) Cation Stabilized by p-

Dimethylaminopyridine or Triphenylphosphane Oxide. *Organometallics* **2013,** *32*, 2406-2415; e) Braunschweig, H.; Celik, M. A.; Dewhurst, R. D.; Heid, M.; Hupp, F.; Sen, S. S. Stepwise isolation of low-valent, low-coordinate Sn and Pb mono- and dications in the coordination sphere of platinum. *Chem. Sci.* **2015,** *6*, 425-435; f) Martincová, J.; Dostál, L.; Herres-Pawlis, S.; Růžička, A.; Jambor, R. Intramolecularly Coordinated [{2,6-(Me2NCH2)2C6H3}SnII]+: A Strong σ Donor for PtII. *Chem. Eur. J.* **2011,** *17*, 7423-7427.

16. a) Filippou, A. C.; Philippopoulos, A. I.; Schnakenburg, G. Triple Bonding to Tin: Synthesis and Characterization of the Square-Pyramidal Stannylyne Complex Cation [(dppe)2W≡Sn−C6H3-2,6-Mes2]+ (dppe = Ph2PCH2CH2PPh2, Mes = C6H2-2,4,6-Me3). *Organometallics* **2003,** *22*, 3339-3341; b) Filippou, A. C.; Portius, P.; Philippopoulos, A. I.; Rohde, H. Triple Bonding to Tin: Synthesis and Characterization of the Stannylyne Complex trans-[Cl(PMe3)4WSnC6H3-2,6-Mes2]. *Angew. Chem. Int. Ed.* **2003,** *42*, 445-447; c) Filippou, A. C.; Ghana, P.; Chakraborty, U.; Schnakenburg, G. Manganese–Tin Triple Bonds: A New Synthetic Route to the Manganese Stannylidyne Complex Cation trans-[H(dmpe)2Mn≡Sn(C6H3-2,6-Mes2)]+ (dmpe = Me2PCH2CH2PMe2, Mes = 2,4,6-Trimethylphenyl). *J. Am. Chem. Soc.* **2013,** *135*, 11525-11528.

17. a) Deolka, S.; Rivada, O.; Aristizábal, S. L.; Fayzullin, R. R.; Pal, S.; Nozaki, K.; Khaskin, E.; Khusnutdinova, J. R. Metal-metal cooperative bond activation by heterobimetallic alkyl, aryl, and acetylide Pt^{II}/Cu^{I} complexes. *Chem. Sci.* **2020,** *11*, 5494-5502; b) Govindarajan, R.; Deolka, S.; Khusnutdinova, J. R. Heterometallic bond activation enabled by unsymmetrical ligand scaffolds: bridging the opposites. *Chem. Sci.* **2022,** *13*, 14008-14031; c) Govindarajan, R.; Deolka, S.; Khaskin, E.; Fayzullin, R. R.; Pal, S.; Vasylevskyi, S.; Khusnutdinova, J. R. H2, B−H, and Si−H Bond Activation and Facile Protonolysis Driven by Pt-Base Metal Cooperation. *Chem. Eur. J.* **2022,** *28*, e202201639.

18. a) Cordovilla, C.; Bartolomé, C.; Martínez-Ilarduya, J. M.; Espinet, P. The Stille Reaction, 38 Years Later. *ACS Catal.* **2015,** *5*, 3040-3053; b) Casado, A. L.; Espinet, P. Mechanism of the Stille Reaction. 1. The Transmetalation Step. Coupling of R1I and R2SnBu3 Catalyzed by trans-[PdR1IL2] (R1 = C6Cl2F3; R2 = Vinyl, 4-Methoxyphenyl; L = AsPh3). *J. Am. Chem. Soc.* **1998,** *120*, 8978-8985.

19. Cabon, Y.; Kleijn, H.; Siegler, M. A.; Spek, A. L.; Gebbink, R. J. M. K.; Deelman, B.-J. Dichlorostannylene complexes of group 10 metals, a unique bonding mode stabilized by bridging 2-pyridyldiphenylphosphine ligands. *Dalton Trans.* **2010,** *39*, 2423-2427.

20. a) Kusumawardani, C.; Permanasari, L.; Fatonah, S. D.; Sugiyarto, K. H. Structural Analysis of Powder Complex of Tris (1,10-phenanthroline) copper(II) Trifluoromethanesulfonate Dihydrate. *Orient. J. Chem.* **2017,** *33*, 2841-2847; b) Harhouri, W.; McHiri, C.; Najmudin, S.; Bonifacio, C.; Nasri, H. Synthesis, FT-IR characterization and crystal structure of aqua(5,10,15,20-tetraphenylporphyrinato-[kappa]4N)manganese(III) trifluoromethanesulfonate. *Acta Crystallographica Section E* **2016,** *72*, 720-723; c) King, R. P.; Herniman, J. M.; Levason, W.; Reid, G. Structural Diversity in Divalent Group 14 Triflate Complexes Involving Endocyclic Thia-Macrocyclic Coordination. *Inorg. Chem.* **2023,** *62*, 853-862; d) The asymmetric stretching modes for SO_3 and CF_3 were observed at 1260 and 1146 cm^{-1}, while those symmetric stretching vibration modes appeared at 1029 and 1223 cm^{-1}, respectively.

21. Spek, A. PLATON SQUEEZE: a tool for the calculation of the disordered solvent contribution to the calculated structure factors. *Acta Crystallogr., Sect. C* **2015,** *71*, 9-18.

22. Hadlington, T. J.; Hermann, M.; Frenking, G.; Jones, C. Low Coordinate Germanium(II) and Tin(II) Hydride Complexes: Efficient Catalysts for the Hydroboration of Carbonyl Compounds. *J. Am. Chem. Soc.* **2014,** *136*, 3028-3031.

23. a) Hadlington, T. J.; Hermann, M.; Li, J.; Frenking, G.; Jones, C. Activation of H_2 by a Multiply Bonded Amido–Digermyne: Evidence for the Formation of a Hydrido–Germylene. *Angew. Chem. Int. Ed.* **2013,** *52*, 10199-10203; b) Khan, S.; Samuel, P. P.; Michel, R.; Dieterich, J. M.; Mata, R. A.; Demers, J.-P.; Lange, A.; Roesky, H. W.; Stalke, D. Monomeric Sn(ii) and Ge(ii) hydrides supported by a tridentate pincer-based ligand. *Chem. Commun.* **2012,** *48*, 4890-4892; c) Pineda, L. W.; Jancik, V.; Starke, K.; Oswald, R. B.; Roesky, H. W. Stable Monomeric Germanium(II) and Tin(II) Compounds with Terminal Hydrides. *Angew. Chem. Int. Ed.* **2006,** *45*, 2602-2605.

24. a) Hadlington, T. J.; Jones, C. A singly bonded amido-distannyne: H2 activation and isocyanide coordination. *Chem. Commun.* **2014,** *50*, 2321-2323; b) Jana, A.; Roesky, H. W.; Schulzke, C.; Döring, A. Reactions of Tin(II) Hydride Species with Unsaturated Molecules. *Angew. Chem. Int. Ed.* **2009,** *48*, 1106-1109.

25. Chai, J.-D.; Head-Gordon, M. Long-range corrected hybrid density functionals with damped atom-atom dispersion corrections. *PCCP* **2008,** *10*, 6615-6620.

26. Weigend, F.; Ahlrichs, R. Balanced basis sets of split valence, triple zeta valence and quadruple zeta valence quality for H to Rn: Design and assessment of accuracy. *PCCP* **2005,** *7*, 3297-3305.

27. Marenich, A. V.; Cramer, C. J.; Truhlar, D. G. Universal Solvation Model Based on Solute Electron Density and on a Continuum Model of the Solvent Defined by the Bulk Dielectric Constant and Atomic Surface Tensions. *J. Phys. Chem. B* **2009,** *113*, 6378-6396.

28. Sindlinger, C. P.; Wesemann, L. Dimeric platinum–stannylene complexes by twofold ligand transfer from an NHC adduct to an organotin(ii) hydride. *Chem. Commun.* **2015,** *51*, 11421-11424.

29. a) Zheng, F.; Hutton, A. T.; van Sittert, C. G. C. E.; Moss, J. R.; Mapolie, S. F. Synthesis, structural characterization and cis–trans isomerization of novel (salicylaldiminato)platinum(ii) complexes. *Dalton Trans.* **2013,** *42*, 11163-11179; b) Romeo, R.; Minniti, D.; Trozzi, M. Uncatalyzed cis-trans isomerization and methanol solvolysis of arylbromobis(triethylphosphine)platinum(II) complexes. A different role for steric hindrance in dissociative and associative mechanisms. *Inorg. Chem.* **1976,** *15*, 1134-1138.

30. Kang, S.-H.; Han, J. S.; Lee, M. E.; Yoo, B. R.; Jung, I. N. Phosphonium Chloride Induced Dichlorosilylene Transfer from Trichlorosilane. *Organometallics* **2003,** *22*, 2551-2553.

31. a) Ghadwal, R. S.; Roesky, H. W.; Merkel, S.; Henn, J.; Stalke, D. Lewis Base Stabilized Dichlorosilylene. *Angew. Chem. Int. Ed.* **2009,** *48*, 5683-5686; b) Ghadwal, R. S.; Azhakar, R.; Roesky, H. W. Dichlorosilylene: A High Temperature Transient Species to an Indispensable Building Block. *Acc. Chem. Res.* **2013,** *46*, 444-456.

32. a) Mitchell, G. P.; Tilley, T. D. Generation of a Silylene Complex by the 1,2-Migration of Hydrogen from Silicon to Platinum. *Angew. Chem. Int. Ed.* **1998,** *37*, 2524-2526; b) Feldman, J. D.; Mitchell, G. P.; Nolte, J.-O.; Tilley, T. D. Isolation and Characterization of Neutral Platinum Silylene Complexes of the Type (R3P)2PtSiMes2 (Mes = 2,4,6-Trimethylphenyl). *J. Am. Chem. Soc.* **1998,** *120*, 11184-11185; c) Waterman, R.; Hayes, P. G.; Tilley, T. D. Synthetic Development and Chemical Reactivity of Transition-Metal Silylene Complexes. *Acc. Chem. Res.* **2007,** *40*, 712-719.

33. Bader, R. F. W. A quantum theory of molecular structure and its applications. *Chem. Rev.* **1991,** *91*, 893-928.

34. Reed, A. E.; Curtiss, L. A.; Weinhold, F. Intermolecular interactions from a natural bond orbital, donor-acceptor viewpoint. *Chem. Rev.* **1988,** *88*, 899-926.

35. Hupp, F.; Ma, M.; Kroll, F.; Jimenez-Halla, J. O. C.; Dewhurst, R. D.; Radacki, K.; Stasch, A.; Jones, C.; Braunschweig, H. Platinum Complexes Containing Pyramidalized Germanium and Tin Dihalide Ligands Bound through σ,σ M□E Multiple Bonds. *Chem. Eur. J.* **2014,** *20*, 16888-16898.

36. a) Cremer, D.; Kraka, E. A description of the chemical bond in terms of local properties of electron density and energy. *Croat. Chem. Acta* **1985,** *57*, 1259-81; b) Macchi, P.; Proserpio, D. M.; Sironi, A. Experimental Electron Density in a Transition Metal Dimer: Metal-Metal and Metal-Ligand Bonds. *J. Am. Chem. Soc.* **1998,** *120*, 13429-13435.

37. a) Lepetit, C.; Fau, P.; Fajerwerg, K.; Kahn, M. L.; Silvi, B. Topological analysis of the metal-metal bond: A tutorial review. *Coord. Chem. Rev.* **2017,** *345*, 150-181; b) Bianchi, R.; Gervasio, G.; Marabello, D. Experimental Electron Density Analysis of Mn2(CO)10: Metal-Metal and Metal-Ligand Bond Characterization. *Inorg. Chem.* **2000,** *39*, 2360-2366.

38. a) Espinosa, E.; Alkorta, I.; Elguero, J.; Molins, E. From weak to strong interactions: A comprehensive analysis of the topological and energetic properties of the electron density distribution involving X-H···F-Y systems. *J. Chem. Phys.* **2002,** *117*, 5529-5542; b) Bader, R. F. W.; Essen, H. The characterization of atomic interactions. *J. Chem. Phys.* **1984,** *80*, 1943-60; c) Bajo, S.; Alférez, M. G.; Alcaide, M. M.; López-Serrano, J.; Campos, J. Metal-only Lewis Pairs of Rhodium with s, p and d-Block Metals. *Chem. Eur. J.* **2020,** *26*, 16833-16845.

39. Saifina, A. F.; Kartashov, S. V.; Saifina, L. F.; Fayzullin, R. R. Applicability of transferable multipole pseudo-atoms for restoring inner-crystal electronic force density fields. Chemical bonding and binding features in the crystal and dimer of 1,3-bis(2-hydroxyethyl)-6-methyluracil. *IUCrJ* **2023,** *10*, 584-602.

40. a) Hunter, G. The exact one-electron model of molecular structure. *Int. J. Quantum Chem* **1986,** *29*, 197-204; b) Shteingolts, S. A.; Stash, A. I.; Tsirelson, V. G.; Fayzullin, R. R. Orbital-Free Quantum Crystallographic View on Noncovalent Bonding: Insights into Hydrogen Bonds, π···π and Reverse Electron Lone Pair···π Interactions. *Chem. Eur. J.* **2021,** *27*, 7789-7809.

41. a) Shteingolts, S. A.; Stash, A. I.; Tsirelson, V. G.; Fayzullin, R. R. Real-Space Interpretation of Interatomic Charge Transfer and Electron Exchange Effects by Combining Static and Kinetic Potentials and Associated Vector Fields**. *Chem. Eur. J.* **2022,** *28*, e202200985; b) Kartashov, S. V.; Shteingolts, S. A.; Stash, A. I.; Tsirelson, V. G.; Fayzullin, R. R. Electronic and Crystal Packing Effects in Terms of Static and Kinetic Force Field Features: Picolinic Acid N-Oxide and Methimazole. *Cryst. Growth Des.* **2023,** *23*, 1726-1742; c) Saifina, A. F.; Kartashov, S. V.; Stash, A. I.; Tsirelson, V. G.; Fayzullin, R. R. Unified Picture of Interatomic Interactions, Structures, and Chemical Reactions by Means of Electrostatic and Kinetic Force Density Fields: Appel's Salt and Its Ion Pairs. *Cryst. Growth Des.* **2023,** *23*, 3002-3018.

42. Bajo, S.; Alcaide, M. M.; López-Serrano, J.; Campos, J. Dehydrogenative Double C−H Bond Activation in a Germylene-Rhodium Complex**. *Chem. Eur. J.* **2021,** *27*, 16422-16428.